J. Fluid Mech. (2011), *vol.* 680, *pp.* 511–533.
doi:10.1017/jfm.2011.176

Modelling nonlinear thermoacoustic instability in an electrically heated Rijke tube

SATHESH MARIAPPAN† AND R. I. SUJITH

Department of Aerospace Engineering, Indian Institute of Technology Madras, Chennai 600036, India

(Received 9 December 2009; revised 4 February 2011; accepted 11 April 2011; first published online 25 May 2011)

An analysis of thermoacoustic instability is performed for a horizontal Rijke tube with an electrical resistance heater as the heat source. The governing equations for this fluid flow become stiff and are difficult to solve by the computational fluid dynamics (CFD) technique, as the Mach number of the steady flow and the thickness of the heat source (compared to the acoustic wavelength) are small. Therefore, an asymptotic analysis is performed in the limit of small Mach number and compact heat source to eliminate the above stiffness problem. The unknown variables are expanded in powers of Mach number. Two systems of governing equations are obtained: one for the acoustic field and the other for the unsteady flow field in the hydrodynamic zone around the heater. In this analysis, the coupling between the acoustic field and the unsteady heat release rate from the heater appears from the asymptotic analysis. Furthermore, a non-trivial additional term, referred to as the global-acceleration term, appears in the momentum equation of the hydrodynamic zone, which has serious consequences for the stability of the system. This term can be interpreted as a pressure gradient applied from the acoustic onto the hydrodynamic zone. The asymptotic stability of the system with the variation of system parameters is presented using the bifurcation diagram. Numerical simulations are performed using the Galerkin technique for the acoustic zone and CFD techniques for the hydrodynamic zone. The results confirm the importance of the global-acceleration term. Bifurcation diagrams obtained from the simulations with and without the above term are different. Acoustic streaming is shown to occur during the limit cycle and its effect on the unsteady heat release rate is discussed.

Key words: aeroacoustics

1. Introduction

Thermoacoustic instability is a challenging problem in solid and liquid rockets, ramjets, aircraft and industrial gas turbines etc. (McManus, Poinsot & Candel 1993). During instability, acoustic oscillations are sustained by the unsteady heat release rate from the heat source (flame) in the combustion chamber, which can cause excessive turbine blade vibration in gas turbines and damage them eventually. Thermoacoustic instability occurs when the acoustic pressure oscillations in the combustion chamber are amplified by the positive feedback of the unsteady heat release rate. A fundamental understanding of the thermoacoustic interaction can be obtained by analysing the thermoacoustic instability in a model problem in a Rijke tube. A Rijke tube is a simple thermoacoustic device, but has much of the essential physics of thermoacoustic

† Email address for correspondence: sathesh.ae@gmail.com

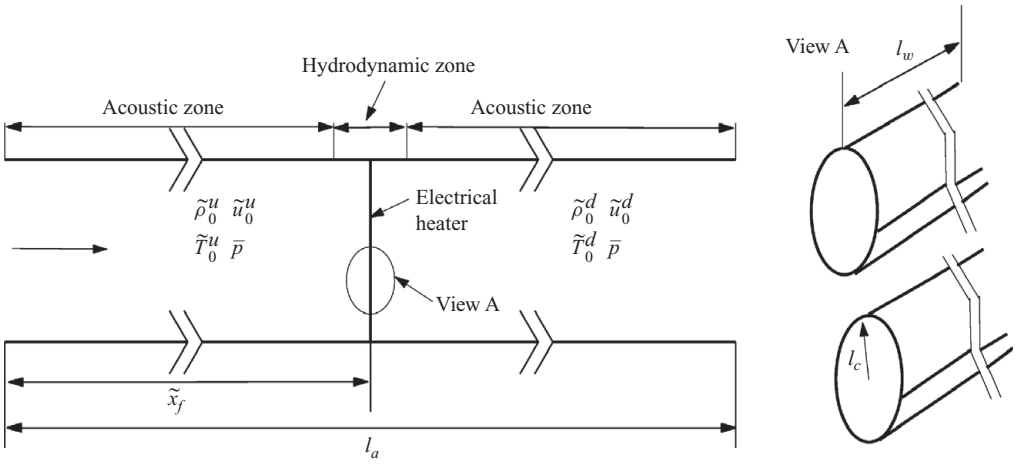

FIGURE 1. Configuration of the Rijke tube showing the acoustic and hydrodynamic zones.

interaction. A Rijke tube is an acoustic resonator tube, with a heat source (in the present case, an electrical heater). The heat source is positioned at some axial location as shown by the configuration of a horizontal Rijke tube in figure 1.

Thermoacoustic instability of Rijke tubes has been studied for a long time. Rijke tube oscillations were first observed by Rijke (1859). He used a vertical tube with a coiled electrical heating filament as the heat source. Self-sustained thermoacoustic oscillations were observed when the heater was positioned at some axial location of the tube and beyond some threshold power level. Rijke gave an explanation based on the pressure pulse generated due to volumetric expansion of the fluid near the heater zone. However, this argument did not explain the fact that instabilities were observed only for some selected range of heater locations. Carvalho *et al.* (1989) employed a linear model for the unsteady heat release rate to calculate the stability of the modes. They applied Rayleigh criteria (Rayleigh 1878) and predicted the axial locations of the heater for which the thermoacoustic oscillations are unstable. However, the above model (Carvalho *et al.* 1989) for the heat source is valid only for small acoustic velocity fluctuations. The stability thus predicted is the linear stability of the system.

For a linearly unstable system, the oscillations grow exponentially, as predicted by the linear stability theory for small amplitudes of oscillations, and eventually reach a limit cycle due to nonlinearities in the heat release rate response of the heater. Nonlinearities in the acoustic field do not contribute to the dynamical evolution of the system as the Mach number ($M \sim 10^{-3}$) of the steady-state flow is very low (Culick 2006). Linear stability theory was further applied to analyse thermoacoustic instability in configurations with multiple heat sources and complex geometries (Bittanti *et al.* 2002). Recently, Heckl & Howe (2007) used Green's function technique to determine the occurrence of thermoacoustic oscillations in a ducted premixed flame.

Estimation of the amplitude of acoustic oscillations during limit cycle is important from the design point of view for gas turbines (Zinn & Lieuwen 2006). In order to achieve this, the nonlinearity in the heat release rate response of the heater has to be accounted for in the model. The nonlinear response of the heater can be determined by solving the governing equations for the fluid flow over the electrical heater, using the computational fluid dynamics (CFD) technique. On the other hand, for low-dimensional modelling, the nonlinear response of the heat source can be obtained from a correlation of the heat transfer between the heater and the local flow velocity

(Heckl 1990). The response of the heat source thus obtained can be considered as a source of acoustic energy, thus coupling the chamber acoustic field with the heat source (Poinsot & Veynante 2005).

A CFD-based analysis was also used to study Rijke tube oscillations. The earliest one was performed by Kwon & Lee (1985). They determined the stability curve for various mean flow rates. Hantschk & Vortmeyer (1999) numerically investigated thermoacoustic oscillations by considering the heat source to be a heated flat plate. They obtained the amplitude and frequency of the thermoacoustic oscillations during the limit cycle. Kopitz & Polifke (2008) used the Nyquist criterion along with CFD to determine the stability of the system. The Nyquist criterion has the advantage of being applicable to complex geometries and non-compact heat sources. Recently, Moeck *et al.* (2009) have numerically investigated thermoacoustic instabilities with the heating source being a flat flame and compared the numerical results with those of experiments.

This extensive analytical and numerical analysis for thermoacoustic instability of a Rijke tube are supplemented by experiments. Matveev & Culick (2003*b*) and Song *et al.* (2006) performed experiments in a horizontal Rijke tube with a mesh-type electrical heating element. The acoustic pressure oscillations were monitored and limit-cycle amplitudes were obtained. For low values of the heater power, the system was stable. As the heater power was increased, the system became linearly unstable and eventually reached a limit cycle.

All the investigations in the analysis of thermoacoustic instability in a Rijke tube described above, except Moeck *et al.* (2009), have used either a response function or solved the Navier–Stokes and energy equations for fluid flow by CFD to obtain the dynamics of the heat source. They assumed a compact heat source (the size of the heat source along the length of the tube is small compared to the acoustic wavelength) and coupled the unsteady heat release rate to the acoustic energy equation as a source. In the above method, the coupling between the chamber acoustic field and the unsteady heat release rate was not obtained with mathematical rigour. Furthermore, there were two systems of equations involved in the problem; one for the acoustic length scale and the other for the length scale of the heat source. They were written and used without mathematical justification. In a rigorous analysis, the above two systems of equations have to be derived from the conservation equations of fluid flow by performing the asymptotic analysis.

Wu *et al.* (2003) have pioneered the application of asymptotic expansions to analyse combustion instabilities. They analysed the amplification of sound waves, when a flame propagates in a gravity field. Separate systems of equations for acoustic field and flame zones were derived, by performing the asymptotic analysis on the conservation equations. They have performed linear-stability analysis for the acoustic–flame coupling, followed by a weakly nonlinear theory for the Darrieus–Landau mode of instability of the flame and the acoustic field. The paper explained the experimental observation of the transition from curved to flat flame during instability. Moeck *et al.* (2007) have also performed the asymptotic analysis to investigate thermoacoustic instability in a Rijke tube with flame as the heat source. They obtained with mathematical rigour the correct systems of equations and the coupling between the acoustic field and the heat source. The presence of an additional global-acceleration term in the momentum equation of the hydrodynamic zone was also observed. Furthermore, they concluded that since one-dimensional (1-D) equations are used in the hydrodynamic zone for their analysis, the above term vanishes, leaving the conventional momentum equation intact in the hydrodynamic zone. The unsteady

heat release rate from the flame may be due to the equivalence ratio fluctuations at the inlet of the hydrodynamic zone, which in turn may be caused by the acoustic velocity at the location of the flame (Moeck *et al.* 2007). Recently, Wu & Moin (2010) investigated the generation of acoustic waves from premixed flame due to free-stream enthalpy fluctuations, using asymptotic analysis. A vigorous subharmonic parametric instability was observed at moderate levels of enthalpy fluctuations.

In the present paper, an investigation of the thermoacoustic instability in an electrically heated Rijke tube is performed starting from the governing equations of fluid flow. An asymptotic analysis (Zeytounian 2002; Ting, Klein & Knio 2007) is then performed in the limit of a compact heat source and zero Mach number of the steady flow to obtain two systems of equations: one governing the acoustic field and the other governing the unsteady flow and heat transfer near the heat source. The separation of equations for the acoustic field and heater (hydrodynamic zone, see figure 1) occurs. The coupling between the above two systems of equations is obtained. Also, the additional global-acceleration term, as obtained by Moeck *et al.* (2007, 2009), appears in the momentum equation for the hydrodynamic zone. It is also found in the present investigation that the presence of global-acceleration term has serious consequences for the bifurcation diagram. The nonlinear evolution equations obtained from the asymptotic analysis in both acoustic and hydrodynamic zones are solved simultaneously. The limit-cycle amplitudes are obtained, which are required to estimate the tolerance limit of the realistic combustors (Zinn & Lieuwen 2006) during instability.

2. Governing equations

The Rijke tube configuration considered here has a length l_a with the heater positioned at an axial location $\tilde{x}_f$ (figure 1). A mean flow is maintained in the tube at a desired flow rate using a blower. The electrical resistance heater, which acts as a heat source, is made up of a thin wire of radius l_c strung around the heater frame. The effective length of the wire filament, which participates in the heat transfer to the fluid flow, is l_w. The typical length of the duct (l_a) is around 1 m and the dimension of the heater along the axial direction of the tube (thickness, l_c) is around 1 mm. The thickness of the heater is very small compared to the length scale of the acoustic field. Hence, the heater can be assumed to be compact compared to the acoustic field in the tube. The zone around the heat source is termed as the hydrodynamic zone. Acoustic and hydrodynamic zones are schematically shown in figure 1.

The length of the hydrodynamic zone in the axial direction is of the order of the thickness of the heater. Hence the hydrodynamic zone can also be assumed to be compact compared to the acoustic field. The heater heats the flow and creates a temperature rise across the heater. Since the heater is compact, piecewise constant steady flow properties can be assumed on either side of the heater (Kaufmann, Nicoud & Poinsot 2002). The Mach number of the flow is $O(10^{-3})$, which leads to a negligible steady-state pressure loss. Hence the steady-state pressure is assumed to be constant along the duct. All upstream steady-state variables are known and specifying any one downstream steady-state variable, such as density (obtained by solving the steady-state version of the equations governing the hydrodynamic zone, which are described in §4.2), is enough to compute the other steady-state variables from the following ideal gas and steady-state continuity equations:

$$\tilde{\rho}_0^d = \frac{\tilde{\rho}_0^u \tilde{T}_0^u}{\tilde{T}_0^d}, \qquad \tilde{u}_0^d = \frac{\tilde{\rho}_0^u \tilde{u}_0^u}{\tilde{\rho}_0^d}, \tag{2.1}$$

where superscripts u and d represent upstream and downstream variables, subscript 0 represents steady-state variables and $\sim$ indicates dimensional variables. The governing equations are

$$\frac{\partial \tilde{\rho}}{\partial \tilde{t}} + \tilde{\nabla}\cdot(\tilde{\rho}\tilde{u}) = 0, \tag{2.2a}$$

$$\tilde{\rho}\left(\frac{\partial}{\partial \tilde{t}} + \tilde{u}\cdot\tilde{\nabla}\right)\tilde{u} + \nabla\tilde{p} = \mu\left(\tilde{\nabla}^2 + \frac{1}{3}\tilde{\nabla}(\tilde{\nabla}\cdot)\right)\tilde{u}, \tag{2.2b}$$

$$\frac{1}{\gamma}\left(\frac{\partial}{\partial \tilde{t}} + \tilde{u}\cdot\tilde{\nabla}\right)\tilde{p} + \tilde{p}\nabla\cdot\tilde{u} = \frac{(\gamma-1)}{\gamma}k\tilde{\nabla}^2\tilde{T}. \tag{2.2c}$$

Non-dimensionalising the above equations using the following scales $\rho = \tilde{\rho}/\bar{\rho}$, $p = \tilde{p}/\bar{p}$, $u = \tilde{u}/\bar{u}$, $T = \tilde{T}/\bar{T}$, $x = \tilde{x}/l_a$, $t_a = \tilde{t}/(l_a/c_0)$, where $\bar{p} = \tilde{p}_0^u = \tilde{p}_0^d$, $\bar{\rho} = \tilde{\rho}_0^u$, $\bar{T} = \bar{p}/(\Re\bar{\rho})$, $\bar{u} = \tilde{u}_0^u$, $c_0 = \sqrt{\gamma\Re\bar{T}}$, $\Re$ is the specific gas constant and c_0 is the local speed of sound, which leads to

$$\frac{\partial \rho}{\partial t_a} + M\nabla_a\cdot(\rho u) = 0, \tag{2.3a}$$

$$\rho\left(\frac{\partial}{\partial t_a} + Mu\cdot\nabla_a\right)u + \frac{1}{\gamma M}\nabla_a p = \frac{M}{Re_a}\left(\nabla_a^2 + \frac{1}{3}\nabla_a(\nabla_a\cdot)\right)u, \tag{2.3b}$$

$$\frac{1}{\gamma}\left(\frac{\partial}{\partial t_a} + Mu\cdot\nabla_a\right)p + Mp\nabla_a\cdot u = \frac{M}{Pe_a}\nabla_a^2 T, \tag{2.3c}$$

where $Re_a = \bar{\rho}\bar{u}l_a/\mu$, $Pe_a = \bar{\rho}\bar{u}l_a C_p/k$, $M = \bar{u}/c_0$, and subscript a indicates that non-dimensionalisation is performed with the acoustic length scale l_a.

An analysis of thermoacoustic instability in a Rijke tube involves the study of a coupled system which consists of the acoustic field in the tube and the unsteady heat transfer from the heat source (hydrodynamic zone). Therefore, it is important to track variations on the length scale of the tube (acoustic scale, $l_a \sim 1$ m) and the length scale of the radius of the heater wire filament ($l_c \sim 1$ mm) in the hydrodynamic zone. Furthermore, the acoustic time scale $t_{ac} = l_a/c_0$ and the wire heat transfer time scale $t_{cc} = l_c/\bar{u}$ are of the same order for typical values mentioned above. This leads to an effective coupling of the dynamics of the acoustic field and the unsteady heat release rate.

The length and time scale ratios are defined as $\delta = l_c/l_a$, $\varepsilon = t_{ac}/t_{cc} = M/\delta \sim 1$. The system has two length scales separated by a large factor ($1/\delta \to \infty$) and a single time scale. Since the flow is at very low Mach number ($M \to 0$), the system of equations (2.3) becomes ill-conditioned (Anderson 2001). Moreover, a smaller grid size near the heater will restrict the maximum time-step that can be allowed for the numerical scheme. All these make (2.3) stiff. As a consequence, solving the problem using the CFD technique is a difficult task. An alternative technique available to solve such a two length-scale problem is the asymptotic analysis (Zeytounian 2002; Ting *et al.* 2007), which is used in the present paper and is discussed in the next section.

3. Asymptotic analysis

In the present investigation, asymptotic analysis is performed in the limit $M \to 0$, $\varepsilon \sim 1$, $\delta \to 0$. The flow variables are expanded in powers of Mach number

(M). The following ansatz for the flow variables is used:

$$\left.\begin{array}{ll} \rho = \rho_s + \rho_c + M\rho_a, & u = u_s + u_a + u_c, \\ p = 1 + Mp_a + M^2 p_c, & T = T_s + T_c + MT_a, \end{array}\right\} \tag{3.1}$$

where subscript s stands for steady-state variables, a for fluctuations due to the acoustic field, and c for fluctuations in the hydrodynamic zone. Here, the acoustic fluctuations exist all along the tube, while the fluctuations due to the heater are confined to a zone around the heater (hydrodynamic zone), which is small compared to the acoustic length scale. Hence the variables with subscript a exist over the length of the tube (acoustic zone, see figure 1), while the variables with subscript c exist only in the region around the heater (hydrodynamic zone, see figure 1) and vanish as one moves away from it. Note that the form of the power series used in ansatz (3.1) is different for various flow variables and the reason is as follows.

The acoustic fluctuations in u are zeroth order in M, whereas the fluctuations in ρ, p, T are first order in M (Rienstra & Hirschberg 2004). On the other hand, temperature fluctuations near the heater (hydrodynamic zone) are comparable to the steady-state temperature T_s and hence T_c appears as a zeroth-order fluctuation (Fu & Tong 2002). The mode of heat transfer from the heater to the gas is by convection. Hence, the zeroth-order fluctuation T_c in temperature (T) is caused by a zeroth-order fluctuation u_c in velocity (u). Because of zeroth-order temperature fluctuations (T_c) and a constant leading-order pressure (3.1), a zeroth-order fluctuation of density (ρ_c) in the hydrodynamic zone is present. (The authors are grateful to an anonymous reviewer for pointing out the errors of the constant density assumption adopted in an earlier version of the paper. The asymptotic analysis is reformulated with the variable density formulation as per the suggestions of the reviewer.) Furthermore, the fluid properties are assumed to be independent of temperature. Now, the ansatz (3.1) is substituted in (2.3) to get the following:

$$\frac{\partial}{\partial t_a}(\rho_s + \rho_c + M\rho_a) + M\nabla_a \cdot ((\rho_s + \rho_c + M\rho_a)(u_s + u_a + u_c)) = 0, \tag{3.2a}$$

$$(\rho_s + \rho_c + M\rho_a)\left(\frac{\partial}{\partial t_a} + M(u_s + u_a + u_c)\cdot\nabla_a\right)(u_s + u_a + u_c) + \frac{1}{\gamma M}\nabla_a(1 + Mp_a + M^2 p_c) = \frac{M}{Re_a}\left(\nabla_a^2 + \frac{1}{3}\nabla_a(\nabla_a \cdot)\right)(u_s + u_a + u_c), \tag{3.2b}$$

$$\frac{1}{\gamma}\left(\frac{\partial}{\partial t_a} + M(u_s + u_a + u_c)\cdot\nabla_a\right)(1 + Mp_a + M^2 p_c) + M(1 + Mp_a + M^2 p_c)\nabla_a \cdot (u_s + u_a + u_c) = \frac{M}{Pe_a}\nabla_a^2(T_s + T_c + MT_a). \tag{3.2c}$$

Initially, equations which are of zeroth order in M are obtained. Then, first-order equations in M are obtained using the solutions from the zeroth-order equations. This process is repeated until governing equations for all the variables in the ansatz (3.1) are obtained. Furthermore, the system of equations for various orders of M is written both for the acoustic and hydrodynamic zones. In the following analysis, equations governing the acoustic zone are first derived and the same exercise is repeated for the hydrodynamic zone.

3.1. *Continuity equation: acoustic zone* $O(M)$

The zeroth-order continuity equation in M reduces to the steady-state equation, which is already used in the analysis (2.1). Collecting terms of first order in M, (3.3) is

obtained. Since the non-dimensionalisation is performed with respect to the acoustic length scale for (2.2), (3.3) represents continuity equation in the acoustic zone:

$$\frac{\partial \rho_a}{\partial t_a} + \nabla_a \cdot ((\rho_s + \rho_c)(u_s + u_a + u_c)) = 0. \tag{3.3}$$

Furthermore, using the continuity equation for steady state in the acoustic zone, $\nabla_a \cdot (\rho_s u_s) = 0$, $\rho_c = 0$ and $u_c = 0$ as described in the ansatz (3.1), (3.3) becomes

$$\frac{\partial \rho_a}{\partial t_a} + \nabla_a \cdot (\rho_s u_a) = 0. \tag{3.4}$$

3.2. *Momentum equation: acoustic zone* $O(M)$

In (3.2*b*), as M is in the denominator of the pressure term, the entire equation is multiplied by M to obtain

$$(M(\rho_s + \rho_c) + M^2 \rho_a)\left(\frac{\partial}{\partial t_a} + M(u_s + u_a + u_c) \cdot \nabla_a\right)(u_s + u_a + u_c) + \frac{1}{\gamma}\nabla_a(1 + Mp_a + M^2 p_c) = \frac{M^2}{Re_a}\left(\nabla_a^2 + \frac{1}{3}\nabla_a(\nabla_a \cdot)\right)(u_s + u_a + u_c). \tag{3.5}$$

The zeroth-order equation in M gives a zero spatial gradient for the steady-state pressure in the system, i.e. $\nabla_a(1) = 0$, where 1 appears due to non-dimensionalisation of $\tilde{p}$ with $\bar{p}$. The condition for constant $\bar{p}$ along the duct is already included in the analysis (2.1). Gathering $O(M)$ terms from (3.5) in the limit $Re_a \to \infty$, leads to the momentum equation in the acoustic zone:

$$\rho_s \frac{\partial u_a}{\partial t_a} + \frac{1}{\gamma}\nabla_a p_a = 0. \tag{3.6}$$

3.3. *Energy equation: acoustic zone* $O(M)$

The zeroth-order terms from (3.2*c*) represent the steady-state energy equation. Since the upstream ($\tilde{T}_0^u$) steady-state temperature is known, steady-state equations governing the heat transfer from the heater are used to obtain the corresponding downstream value ($\tilde{T}_0^d$), thus making the collection of $O(1)$ terms from (3.2*c*) redundant. Now the $O(M)$ terms are gathered to obtain the acoustic energy equation:

$$\frac{1}{\gamma}\frac{\partial p_a}{\partial t_a} + \nabla_a \cdot u_a = \frac{1}{Pe_c \delta}\nabla_c^2 T_c, \tag{3.7}$$

where $Pe_c = \bar{\rho}\bar{u}l_c C_p/k$. The unsteady heat release rate from the heater is delivered into the acoustic zone by local thermal conduction. Hence, the last term in (3.7) represents the coupling term from the hydrodynamic to the acoustic zone. Assuming a one-dimensional acoustic field in the axial direction x_a, (3.7) is integrated over the cross-sectional area (S_c) of the tube. In order to convert from 3-D to 1-D space, the terms with gradients (∇_a) in the acoustic length scale are replaced by $\partial/\partial x_a$ in (3.7). The acoustic energy equation takes the following form:

$$S_c\left(\frac{1}{\gamma}\frac{\partial p_a}{\partial t_a} + \frac{\partial u_a}{\partial x_a}\right) = \frac{1}{Pe_c \delta}\left(\iiint_{V_c} \nabla_c^2 T_c \, \mathrm{d}\tilde{V}_c\right)\hat{\delta}(\tilde{x} - \tilde{x}_f), \tag{3.8}$$

where V_c is the volume of the hydrodynamic zone and $\hat{\delta}(x)$ is the Dirac delta function, which is used to indicate the compactness of the hydrodynamic zone in

the equations. The volume integral is converted into a surface integral using Gauss's divergence theorem. In order to apply the above theorem, the last term in (3.8) is dimensionalised, followed by the application of the Gauss divergence theorem and again non-dimensionalised back to get the following acoustic energy equation:

$$\frac{1}{\gamma}\frac{\partial p_a}{\partial t_a}+\frac{\partial u_a}{\partial x_a}=\frac{l_w l_c}{Pe_c S_c}\left(\int_0^{2\pi}(-\nabla_c T_c)_{\hat{e}_r}\,\mathrm{d}\theta\right)\widehat{\delta}(x-x_f), \tag{3.9}$$

where l_w is the length of the wire which contributes to the heat transferred to the fluid, $\hat{e}_r$ is the unit vector along the radial direction from the cylinder surface, $(\nabla_c T_c)_{\hat{e}_r}$ represents the component of gradient of T_c along $\hat{e}_r$. The term on the right-hand side of (3.9) is identified as the coupling term from hydrodynamic zone to the acoustic zone, which drives the acoustic oscillations in a Rijke tube. The unsteady heat release rate from the hydrodynamic zone is given by $q=(l_w l_c/Pe_c S_c)(\int_0^{2\pi}(-\nabla_c T_c)_{\hat{e}_r}\,\mathrm{d}\theta)$ with the integral evaluated over surface of the cylinder. The equations governing the acoustic zone are thus obtained and the coupling of the acoustic field with the unsteady heat release rate of the heater appears from the asymptotic analysis. The equations for the hydrodynamic zone are derived in the following subsections.

3.4. *Continuity equation: hydrodynamic zone* $O(1)$

In order to obtain the equations with respect to the hydrodynamic zone, the spatial derivatives in the acoustic length scale (l_a) have to be converted to the length scale (l_c) of the heater, only for variables with subscript c. The transformation $\nabla_a=\nabla_c/\delta$ is applied to (3.2). The subscript c in ∇ operator represents the derivatives that are non-dimensionalised with l_c. During the scale change from l_a to l_c, terms which are second order in M, for e.g. $M^2\nabla_a$, become first order in M, $M\varepsilon\nabla_c$. The inclusion of such terms leads to the continuity equation in the hydrodynamic zone as follows:

$$\frac{\partial}{\partial t_c}(\rho_s+\rho_c)+\nabla_c\cdot((\rho_s+\rho_c)(u_s+u_c+u_a|_{x_f}))=0, \tag{3.10}$$

where $u_a|_{x_f}$ represents u_a at the non-dimensionalised heater location x_f ($x_f=\tilde{x}_f/l_a$) and $\partial/\partial t_c=(1/\varepsilon)\partial/\partial t_a$. In (3.10), $\rho_s+\rho_c$ and $u_s+u_c+u_a|_{x_f}$ appear effectively as one variable. Hence, the following change of variables $\rho_p=\rho_s+\rho_c$ and $u_p=u_s+u_c+u_a|_{x_f}$ is applied in (3.10) to obtain

$$\frac{\partial\rho_p}{\partial t_c}+\nabla_c\cdot(\rho_p u_p)=0, \tag{3.11}$$

which is the conventional continuity equation for flows of variable density fluid.

3.5. *Momentum equation: hydrodynamic zone* $O(1)$

The zeroth-order momentum equation in the hydrodynamic zone is as follows:

$$\begin{aligned}&(\rho_s+\rho_c)\left(\frac{\partial}{\partial t_c}+(u_a|_{x_f}+u_s+u_c)\cdot\nabla_c\right)(u_a|_{x_f}+u_s+u_c)\\&\quad+\frac{1}{\gamma}\nabla_c p_c=\frac{1}{Re_c}\left(\nabla_c^2+\frac{1}{3}\nabla_c(\nabla_c\cdot)\right)(u_a|_{x_f}+u_s+u_c)-\frac{1}{\varepsilon}\nabla_a\left(\frac{p_a}{\gamma}\right)\Big|_{x_f},\\&\quad\text{Boundary condition (BC): } u_c\to 0,\ \text{as } x_c\to\infty,\end{aligned} \tag{3.12}$$

where $Re_c=\bar{\rho}\bar{u}l_c/\mu$ and $\nabla_a(p_a/\gamma)|_{x_f}$ represents $\nabla_a(p_a/\gamma)$ evaluated at x_f. The equations are then written in terms of ρ_p and u_p and the acoustic momentum

equation (3.6) is used to replace the last term in (3.12), to obtain

$$\rho_p \left(\frac{\partial}{\partial t_c} + u_p \cdot \nabla_c \right) u_p + \frac{1}{\gamma} \nabla_c p_c = \frac{1}{Re_c} \left(\nabla_c^2 + \frac{1}{3} \nabla_c (\nabla_c \cdot) \right) u_p + \rho_s \left. \frac{\partial u_a}{\partial t_c} \right|_{x_f},$$
$$\text{BC: } u_p \to u_s + u_a|_{x_f}, \text{ as } x_c \to \infty, \tag{3.13}$$

where $\partial u_a/\partial t_c|_{x_f}$ represents $\partial u_a/\partial t_c$ evaluated at the non-dimensional heater location x_f. Note that (3.13) is the momentum equation for unsteady variable density flow over the heater, with an additional term $\partial u_a/\partial t_c|_{x_f}$. The above additional term is referred to as the global-acceleration term (Moeck *et al.* 2009), which can be identified as a coupling term for the momentum equation in the hydrodynamic zone from the acoustic zone, apart from that due to the boundary condition associated with (3.13).

The global-acceleration term occurs in two length-scale problems (Klein 1995; Klein *et al.* 2001). This term would not have been identified had the asymptotic analysis not been performed. In most thermoacoustic systems, there are at least two length scales: the length scale of the acoustic field and the length scale of the heat source. Therefore, the above term is expected to be present in the analysis of thermoacoustic systems. The same term can be interpreted as the pressure gradient imposed by the acoustic field on the hydrodynamic zone (Ting *et al.* 2007). Note that if one performs response function calculations numerically (for example Preetham, Santosh & Liewen 2008) for the unsteady heat release rate from the heater, where no acoustic field is imposed, then $\partial u_a/\partial t_c|_{x_f}$ will not be anticipated and hence will not be included. This leads to solving an incorrect system of equations and prediction of the dynamics of thermoacoustic interaction in a Rijke tube system. Numerical simulations are performed with and without the global-acceleration term in the present paper. It is observed that the error due to neglecting the above term is large and predictions of the dynamical evolution of the system are modified to a large extent. This observation has been emphasised in § 5.2.

3.6. *Energy equation: hydrodynamic zone* $O(1)$

Since the temperature fluctuations due to the heater are zeroth order in M as explained in the ansatz (3.1), $O(1)$ terms are gathered from (3.2*c*) to obtain

$$\nabla_c \cdot (u_s + u_a|_{x_f} + u_c) = \frac{1}{Pe_c} \nabla_c^2 (T_s + T_c). \tag{3.14}$$

A change of variable $T_p = T_s + T_c$ is performed in (3.14) leading to

$$\nabla_c \cdot u_p = \frac{1}{Pe_c} \nabla_c^2 T_p,$$
$$\text{BC: } \nabla_c T_p \to 0, \text{ as } x_c \to \infty, \text{ and } T_p = \tilde{T}_w/\bar{T}, \; x_c = \text{cylinder surface}, \tag{3.15}$$

where $\tilde{T}_w$ represents the surface temperature of the heater wire. The energy equation (2.3*c*) simplifies to an algebraic constraint (3.15) on the velocity field u_p. The amount of local dilatation of the fluid is governed by (3.15). Integration of the same equation over the hydrodynamic zone gives the net dilatation in the volume of the fluid as it passes through the hydrodynamic zone. The presence of the heat source which leads to the dilatation in the volume of the fluid manifests as the acoustic velocity jump ($u_a|_{x_f}$) across the heat source. This in turn drives the acoustic field in the tube. The above argument is consistent with the derivation of the acoustic energy equation described in § 3.3, where the Dirac delta function in (3.9) causes the acoustic velocity jump across x_f. Thus, the acoustic velocity jump is used as the matching condition

across the hydrodynamic zone. The above conclusion is independent of the type of the heat source and the interpretation is valid as long as the heat source can be considered as compact with respect to the acoustic field.

In multiple-scale asymptotics, averaging the flow variables over the small-scale hydrodynamic zone is performed to obtain the flow variables in the large-scale acoustic zone (Klein *et al.* 2001). Accordingly, the term $\partial u_a/\partial t_c|_{x_f}$ in (3.13) is evaluated as the average of the values at the upstream and downstream locations of the heat source, due to acoustic velocity jump. Averaging the momentum equation of the hydrodynamic zone (3.13) leads to acoustic momentum equation (3.6) defined at the heat source, with the acoustic velocity obtained as the average of u_a upstream and downstream of the heat source. The same averaging procedure is performed for the global acceleration term as well, which is used in (3.13). The system of equations for the hydrodynamic zone (3.11), (3.13) and (3.15) is not closed. The ideal gas equation is used to obtain the relation between ρ_p and T_p in the hydrodynamic zone as follows:

$$(1 + Mp_a + M^2 p_c) = (\rho_s + \rho_c + M\rho_a)(T_s + T_c + MT_a). \tag{3.16}$$

Equating the zeroth-order terms gives the following:

$$\rho_p = \frac{1}{T_p}. \tag{3.17}$$

Solving (3.15) simultaneously with (3.11), (3.13) and (3.17) gives the temperature field T_p. The unsteady heat release rate $q = (l_w l_c / Pe_c S_c)[(\int_0^{2\pi} -\nabla_c (T_p - T_s)_{\hat{e}_r} \mathrm{d}\theta)]$ is then obtained from T_p. This q serves as the source term for (3.9).

4. Solution technique

The governing equations in the acoustic and hydrodynamic zones are solved using different solution techniques. First, the solution technique used in the acoustic zone is discussed.

4.1. *Equations governing the acoustic zone: one-dimensional form*

The acoustic continuity (3.4) and momentum (3.6) equations are converted from 3-D to 1-D space as described in § 3.3. The governing equations thus obtained for the acoustic zone are as follows:

$$\rho_s \frac{\partial u_a}{\partial t_a} + \frac{1}{\gamma}\frac{\partial p_a}{\partial x_a} = 0, \tag{4.1a}$$

$$\frac{1}{\gamma}\frac{\partial p_a}{\partial t_a} + \frac{\partial u_a}{\partial x_a} = q\hat{\delta}(x - x_f). \tag{4.1b}$$

The above partial differential equations (4.1*a*, *b*) are converted to ordinary differential equations (ODEs) by the Galerkin technique (Zinn & Lores 1971; Padmanabhan 1975). In the Galerkin technique, the unknown variables are expanded using basis functions, which satisfy the boundary conditions. In the present paper, the Rijke tube considered is open at both ends. The basis functions are chosen accordingly to satisfy the acoustic boundary conditions. The acoustic variables u_a and p_a are expanded in terms of the basis function as follows:

$$p_a = \gamma \sum_{m=1}^{N} P_m \sin(\omega_m x), \qquad u_a = \sum_{m=1}^{N} U_m \cos(\omega_m x), \tag{4.2}$$

where $\omega_m = m\pi$, N is the number of modes chosen in the Galerkin expansion. The dynamical evolution equation for P_m and U_m is obtained by projecting (4.1) on

to the Galerkin basis, after substituting the expansion for p_a and u_a from (4.2). The application of the Galerkin technique to the present problem is similar to that performed by Balasubramanian & Sujith (2008). The final ODEs are of the following form:

$$\sum_{m=1}^{N} \left(\rho_s^u I_{m,n}^u - \rho_s^d I_{m,n}^d\right) \dot{U}_m + P_n \omega_n = 0, \tag{4.3a}$$

$$\dot{P}_n - \omega_n U_n + \zeta_n \omega_n P_n = 2q \sin(\omega_n x_f), \tag{4.3b}$$

where

$$I_{m,n}^u = \rho_s^u \begin{cases} \dfrac{\sin((\omega_m + \omega_n)x_f)}{\omega_m + \omega_n} + \dfrac{\sin((\omega_m - \omega_n)x_f)}{\omega_m - \omega_n}, & \omega_m \neq \omega_n, \\ \dfrac{\sin(2\omega_n x_f)}{2\omega_n} + x_f, & \omega_m = \omega_n, \end{cases} \tag{4.4}$$

$$I_{m,n}^d = \rho_s^d \begin{cases} \dfrac{\sin((\omega_m + \omega_n)(1 - x_f))}{\omega_m + \omega_n} + \dfrac{\sin((\omega_m - \omega_n)(1 - x_f))}{\omega_m - \omega_n}, & \omega_m \neq \omega_n, \\ 1 - \dfrac{\sin(2\omega_n x_f)}{2\omega_n} - x_f, & \omega_m = \omega_n, \end{cases} \tag{4.5}$$

where $\zeta_n = (C_1(\omega_n/\omega_1) + C_2\sqrt{\omega_1/\omega_n})/(2\pi)$, $\omega_n = n\pi$, and ζ_n represents damping in the acoustic zone due to viscosity and end losses. Here, C_1, C_2 are the coefficients that determine the amount of damping and whose numerical value is given by Matveev & Culick (2003*a*). The system of equations (4.3) is solved using the fourth-order Runge–Kutta (RK4) method (Riley *et al.* 2006). The value of the unsteady heat release rate q is obtained at each substep of RK4 by solving the equations corresponding to the hydrodynamic zone (4.6), which is discussed in the following section.

4.2. *Equations governing the hydrodynamic zone*

The governing equations for the hydrodynamic zone are summarised below:

$$\frac{\partial \rho_p}{\partial t_c} + \nabla_c \cdot (\rho_p u_p) = 0, \tag{4.6a}$$

$$\rho_p \left(\frac{\partial}{\partial t_c} + u_p \cdot \nabla_c\right) u_p + \frac{1}{\gamma} \nabla_c p_c = \frac{1}{Re_c} \left(\nabla_c^2 + \frac{1}{3} \nabla_c (\nabla_c \cdot)\right) u_p + \rho_s \left.\frac{\partial u_a}{\partial t_c}\right|_{x_f}, \tag{4.6b}$$

$$\nabla_c \cdot u_p = \frac{1}{Pe_c} \nabla_c^2 T_p, \tag{4.6c}$$

$$\rho_p = \frac{1}{T_p}. \tag{4.6d}$$

As described in § 2, the heater in its primitive form is a thin wire filament. To simulate the dynamics of the heater, Selimefendigil, Föller & Polifke (2008) have analysed the unsteady convective heat transfer from a heated circular cylinder. Following this approach, the above system of equations (4.6) is solved for the unsteady convective heat transfer over the circular cylindrical heated wire filament. The flow field over the heater wire filament is assumed to be two-dimensional. The governing equations are solved by CFD. The details of the geometry of the heat source and the boundary conditions imposed on the hydrodynamic zone are discussed in the Appendix. The unsteady heat release rate q is obtained from the temperature field T_p. The obtained q is then used as the source term for (4.3*b*) at each substep of RK4, as described

Acoustic zone	Hydrodynamic zone	CFD simulations
$l_a = 1$ m, $S_c = 0.01$ m^2	$Re_d = 20$	Number of grids $(r, \theta) = 100 \times 120$
$\bar{P} = 1$ bar	$l_c = 2.6$ mm	Residue for continuity $= 10^{-6}$
$\tilde{\rho}_0^u = 1.18$ kg m^{-3}	$l_w = 10$ m	Residue for momentum $= 10^{-6}$
$\tilde{T}_0^u = 295$ K	$\tilde{T}_w = 700$ K	Residue for energy $= 10^{-6}$
$\tilde{\rho}_0^d = 0.84$ kg m^{-3}	$M = 5 \times 10^{-4}$	$\Delta t_a = 5 \times 10^{-4}$

TABLE 1. Physical parameters in acoustic zone, hydrodynamic zone and numerical parameters used for CFD simulations.

in § 4.1. Thus, the system of equations in the acoustic (4.3) and hydrodynamic zones (4.6) is solved simultaneously.

5. Results and discussions

Numerical simulations are performed with the parameters shown in table 1. In the following simulations, the number of the Galerkin modes is chosen as $N = 100$ (to capture the acoustic velocity jump across the heat source), such that a further increase in N leads to less than 5 % variation in the results. Unless otherwise specified, the parameter values in table 1 are used for the simulations. The numerical values of the damping coefficients used for the present simulations are $C_1 = 0.27$ and $C_2 = 0.03$ (Matveev & Culick 2003*a*). In the acoustic zone upstream and downstream of the heater, one-dimensional governing equations are used. The hydrodynamic zone equations in the present case are solved in a two-dimensional domain (see the Appendix). Hence, the density ($\tilde{\rho}_d^0$) in the hot side of the acoustic zone is obtained by averaging the steady-state density ρ_s at the far downstream end of the hydrodynamic zone. The value of $\tilde{\rho}_d^0$ thus obtained is listed in table 1.

5.1. *Stability regimes*

The experimental results of Matveev & Culick (2003*b*) indicate that the system becomes linearly unstable beyond some critical value of the heater power. As the heater power is increased, the present numerical simulations show two stability regimes: a linearly stable regime and a linearly unstable regime. The non-dimensional heater power (K) is defined as $K = (l_w l_c)/(Pe_c S_c)$ (see § 3.6 for the expression of q). The average of the acoustic velocity upstream and downstream of the heat source is taken as the acoustic velocity (u_f) at the heat source. In the subsequent sections, the variables u_f and q are considered as the representative variables to illustrate the dynamical behaviour of the system in the acoustic and hydrodynamic zones, respectively. The subsequent sections discuss the results of the numerical simulation.

5.1.1. *Linearly stable regime*

For low values of the heater power K, the system is stable to small-amplitude initial perturbations. In figure 2(*a*), the initial perturbation in acoustic velocity ($u_f = u_a|_{x_f}$) at the heater location is around 5 % of the mean flow velocity. The perturbation decays to zero in the asymptotic time limit. The phase plot between u_f and the non-dimensional fluctuating heat release rate (q) shows the evolution of the system in figure 2(*b*) towards a stable focus. The arrows indicate the direction of the evolution of the system in the phase plane.

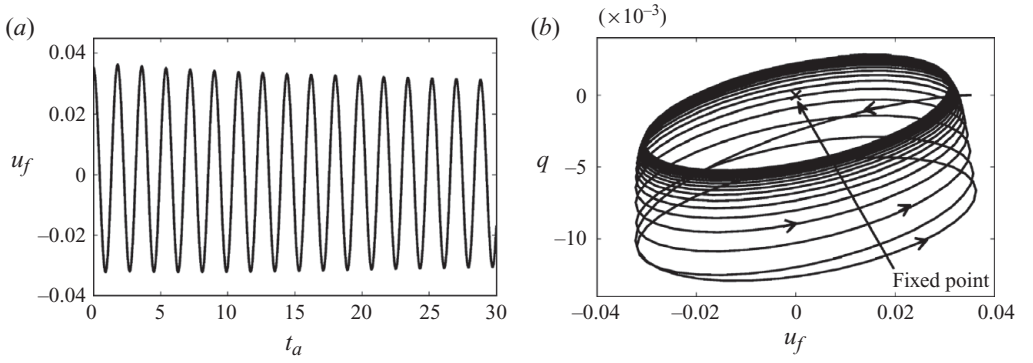

FIGURE 2. The linearly stable system: (*a*) evolution of the acoustic velocity (u_f) at the heater location (x_f); (*b*) phase portrait between u_f and unsteady heat release rate q, $x_f = 0.25$, $K = 0.10$, $U_1(t=0) = 0.05$, $U_{m\neq 1}(t=0) = 0$ and $P_m(t=0) = 0$.

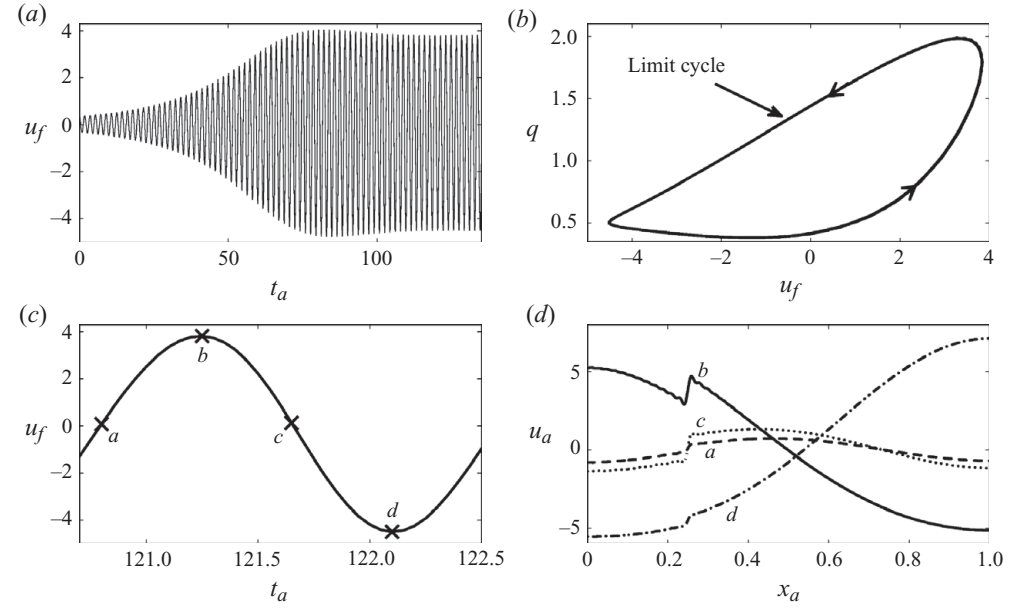

FIGURE 3. The linearly unstable system: (*a*) evolution of the acoustic velocity (u_f) at the heater location (x_f); (*b*) phase portrait between u_f and unsteady heat release rate q (only limit cycle is shown, transients are not shown for clarity); (*c*) evolution of u_f during a period of the limit cycle; (*d*) distribution of the acoustic velocity u_a in the Rijke tube during a period of the limit cycle. $x_f = 0.25$, $K = 0.1785$, $U_1(t=0) = 0.5$, $U_{m\neq 1}(t=0) = 0$ and $P_m(t=0) = 0$.

5.1.2. *Linearly unstable regime*

In the second stability regime, the system is unstable for small-amplitude perturbation, $u_f(t=0) = 0.4$, which is 10 % of the limit-cycle amplitude (see figure 3*a*). The figure shows that u_f grows exponentially, eventually reaching a limit cycle. The limit cycle is a closed curve in the phase portrait as shown in figure 3(*b*). The acoustic velocity (u_a) distribution along the duct at various instances over a period, as marked in figure 3(*c*), is shown in figure 3(*d*). It is observed that the acoustic velocity jump

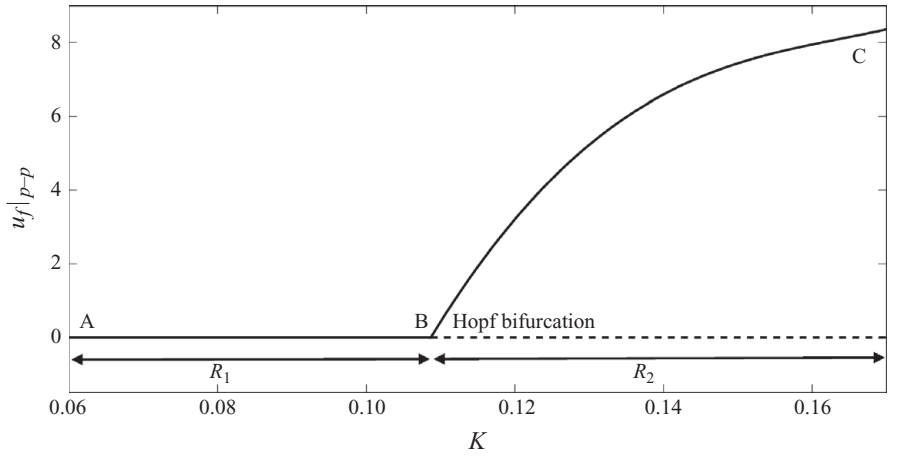

FIGURE 4. Bifurcation diagram with the non-dimensional heater power K as the control parameter. The other parameters are $x_f = 0.25$. The two regimes are R_1, linearly stable regime, and R_2, linearly unstable regime.

is captured by the Galerkin technique. The stability regimes of a system with the variation of a parameter can be represented using a bifurcation diagram.

5.1.3. *Bifurcation diagram*

Simulations are performed with the heater power as the control parameter and the peak-to-peak value of acoustic velocity ($u_f|_{p-p}$) at the heater location (x_f) in the asymptotic time limit is chosen as the representative variable. The resolution in the control parameter K for figure 4 is 2×10^{-3}, which is 1.8 % of the value of $K = 0.11$ at the Hopf point (B). In the bifurcation diagram shown in figure 4, solid lines indicate stable solutions, while the dashed line indicates unstable solutions. For low values of K (say, $K = 0.06$), the asymptotic state ($u_f = 0$) is the stable fixed point. This corresponds to the first stability regime (§5.1.1), where the system is linearly stable. As the heater power is increased, beyond point 'B' ($K = 0.11$), the system becomes linearly unstable and reaches a limit cycle. The above transition happens via Hopf bifurcation. Also, the amplitude of the limit cycle increases as the heater power is increased further. This corresponds to the second stability regime.

5.2. *Effect of global acceleration on the stability of the system*

An asymptotic analysis is performed to obtain separate systems of equations governing the dynamics in the acoustic and hydrodynamic zones. The critical outcome of the above analysis is the presence of the additional term $\partial u_a/\partial t_c|_{x_f}$ in (3.13). The importance of the global-acceleration term is shown in figure 5. In figure 5(a), evolution of u_f is shown with and without this term for identical system parameters and initial conditions. The system parameters are chosen such that the simulation performed is in the linearly unstable regime ($K = 0.1785$, see figure 4). With the initial perturbation $U_1(t = 0) = 0.5$, the simulation with the $\partial u_a/\partial t_c|_{x_f}$ term indicates that the system reaches a limit cycle eventually. The evolution of the system to a limit cycle is shown in the inner figure 5(b). However, for the same system parameters and initial conditions, if the above term is dropped from (3.13), the simulation indicates that the system reaches a stable focus in the asymptotic time limit.

To analyse the behaviour of the system in the absence of the global-acceleration term, the bifurcation diagram is computed without the term $\partial u_a/\partial t_c|_{x_f}$ in (3.13),

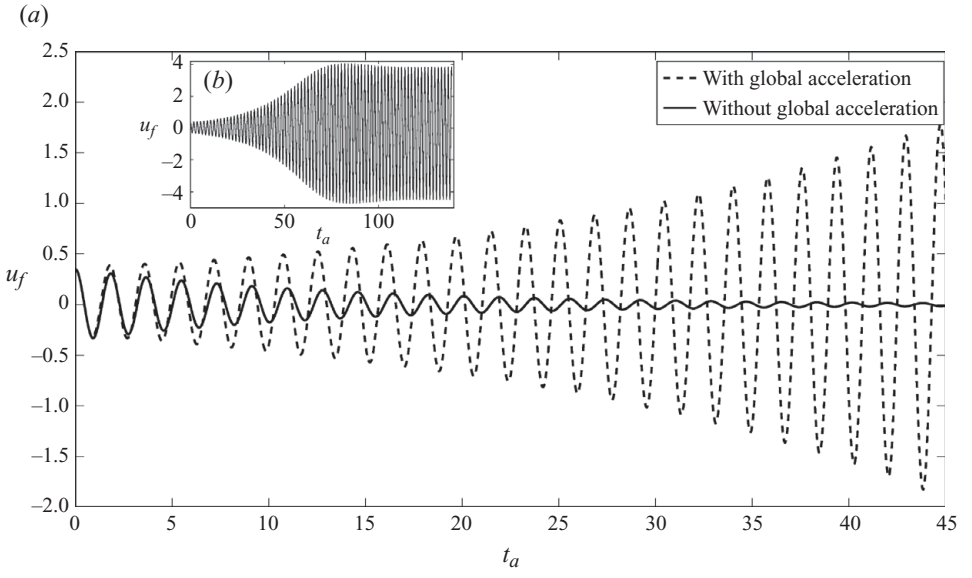

FIGURE 5. (*a*) Comparison of the evolution of acoustic velocity (u_f) at the heater location (x_f) with and without the global-acceleration term in (3.12). (*b*) Evolution of u_f for a longer period of time with the global-acceleration term, 'zoomed out' view of (*a*). $x_f = 0.25$, $K = 0.1785$, $U_1(t=0) = 0.5$, $U_{m\neq1}(t=0) = 0$ and $P_m(t=0) = 0$.

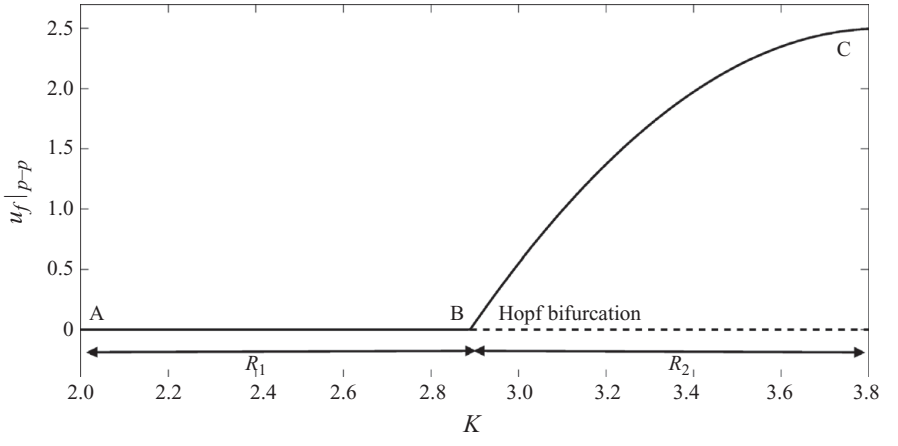

FIGURE 6. Bifurcation diagram with non-dimensional heater power K as the control parameter without the global-acceleration term in (3.12). The parameters chosen are the same as for the simulation shown in figure 4.

as shown in figure 6. A significant difference between the bifurcation diagram with and without the inclusion of the global-acceleration term is that the system becomes linearly unstable at $K = 0.11$ (see figure 4) for the simulation performed with the global-acceleration term, whereas the same behaviour happens at $K = 2.89$ (see figure 6) for the simulation performed without the same term. The numerical simulation without the global-acceleration term predicts linear instability at a value of K which is one order of magnitude higher than that obtained from the numerical

simulation with the inclusion of the same term. The term $\partial u_a/\partial t_c|_{x_f}$ acts as a forcing term for (3.13) from the acoustic zone. Hence, dropping the above term breaks the feedback from the acoustic to the hydrodynamic zone apart from the feedback from the free-stream boundary condition for (3.13). The strength of the feedback loop between the acoustic and hydrodynamic zones is thus weakened. Therefore, it is important to perform the asymptotic analysis to obtain the correct system of equations for the two zones in solving the two length-scale problems.

An analysis of thermoacoustic instability using the response function (to capture the dynamics of the heat source) is termed as a two-part approach (Candel 2002). In this approach, the response function of the heat source to velocity fluctuations is first obtained. The response function thus obtained is used in the acoustic energy equation. The acoustic equations are then solved with the appropriate boundary conditions and the stability of the system is determined. When the response function is obtained numerically (see for example Preetham *et al.* (2008)), the global-acceleration term is not taken into account in the governing equations for the dynamics of the heat source. If the prediction of thermoacoustic instability is performed based on the response function of the heat source, the effect of the above term is absent. As a consequence, the coupling between the acoustic and hydrodynamic zones is weakened, which leads to overprediction of the stability of the thermoacoustic system.

Furthermore, it is important to analyse the dynamics of the system in the asymptotic time limit. As fluid convection is the source of energy transfer from the heated wires to the flow, the flow field during a limit cycle will reveal important insights about them.

5.3. *Unsteady flow field in the hydrodynamic zone*

The flow field in the hydrodynamic zone during a limit cycle is investigated in this section. Figure 7 shows the streamlines of the velocity field u_p for the flow over the heater wire at various instants of a limit cycle. Only one half of the flow field is shown in the figure due to the symmetry condition (see the Appendix). The acoustic velocity $u_a|_{x_f}$ at the heater location ranges from -4 to $+4$ during one period of the limit cycle (figure 7*f*). Hence, during the first half of the limit cycle, the flow is from left to right, and during the next half it is from right to left. A complete flow reversal in the free stream happens, as shown in figure 7(*a–e*). Labels (*a–e*) illustrated in figure 7(*f*) indicate the flow field at various instants of the acoustic velocity ($u_a|_{x_f}$) shown in figure 7(*a–e*).

When $u_a|_{x_f} = 0$ (figure 7*a*), the flow field resembles the steady flow over the cylinder. As $u_a|_{x_f}$ increases and reaches a maximum, the recirculation zone is pushed further downstream (figure 7*b*) and during subsequent time, $u_a|_{x_f}$ decreases, followed by flow reversal in the free-stream direction (figure 7*e*). Thus, the fluctuations in the velocity field (u_p) during the limit cycle are comparable to the steady base flow (u_s). Hence, nonlinear effects such as steady streaming (Telionis 1981) will be predominant.

In the present case, since the acoustic velocity (u_a) is responsible for flow oscillation in the hydrodynamic zone, the steady streaming thus obtained is termed as acoustic streaming (Andres & Ingard 1953).

Figure 8(*a–c*) shows the effects of acoustic streaming during the limit cycle. Figure 8(*a*) shows the averaged streamlines of u_p during one period of the limit cycle (figure 7*f*). The streamlines of the steady-state flow u_s are shown in figure 8(*b*). There are visible differences between figures 8(*a*) and 8(*b*), and hence, apart from the steady base flow, a non-zero mean flow arises during the limit cycle due to the nonlinearity. The streamlines obtained from the difference of the above two flow fields (figure 8(*a*, *b*) are shown in figure 8(*c*). The streamlines are slightly tilted towards the

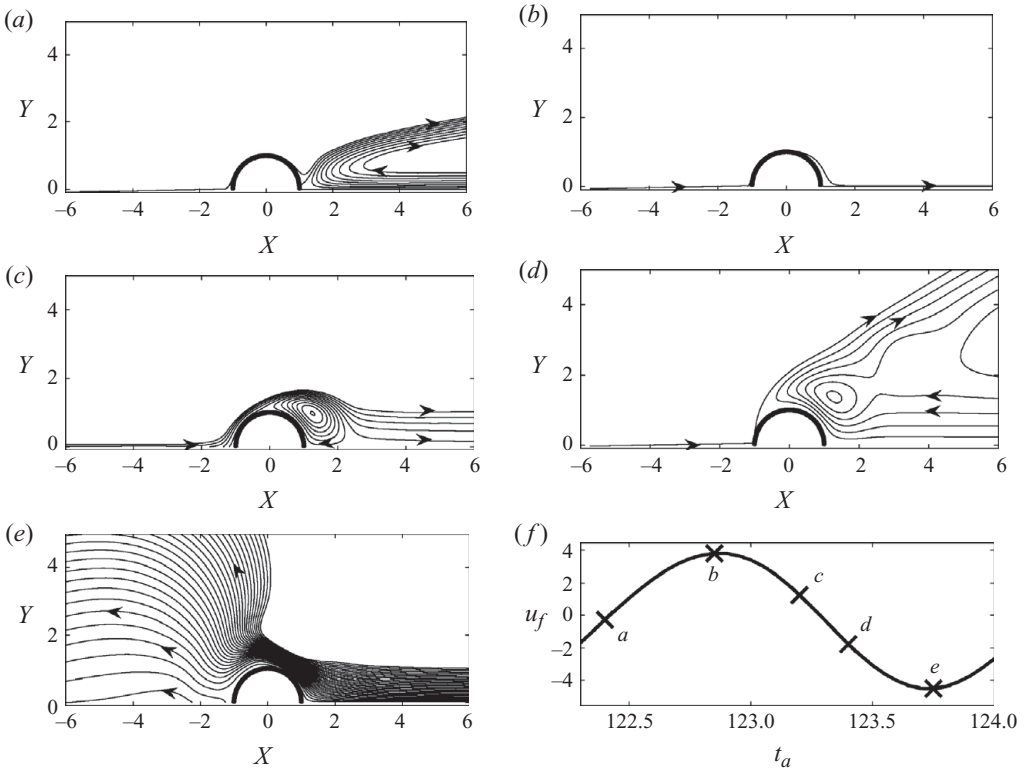

FIGURE 7. Streamlines (*a–e*) in the hydrodynamic zone (corresponding to u_p) at various instants during one period of the limit cycle; (*f*) evolution of u_a at x_f during a limit cycle; $K = 0.1785$, $x_f = 0.25$ and $l_w = 10$ m.

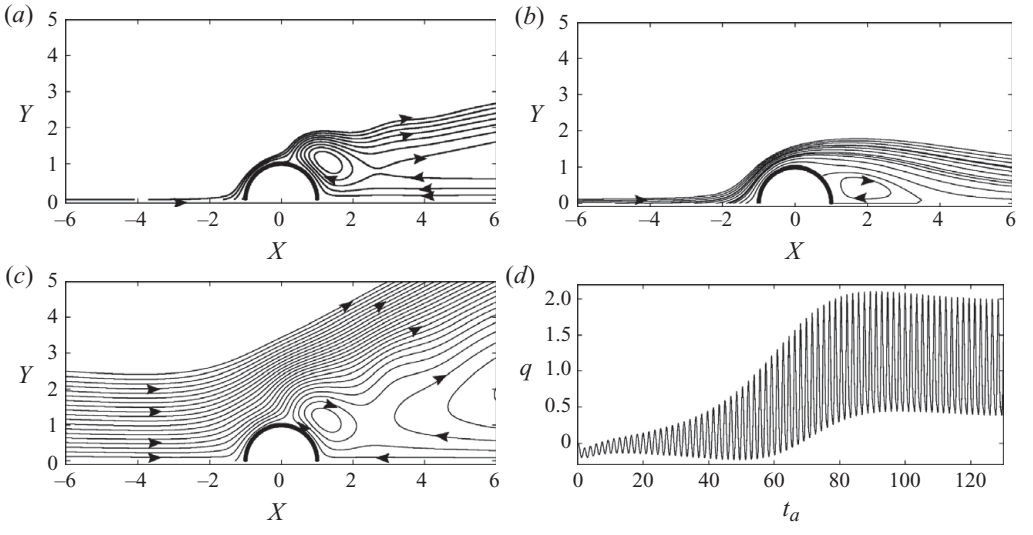

FIGURE 8. Flow streaming in the hydrodynamic zone: (*a*) streamlines averaged over one period of the limit cycle; (*b*) streamlines of the steady base flow; (*c*) streamlines of the velocity difference between (*a*) and (*b*); (*d*) evolution of the non-dimensional unsteady heat release rate (q), showing a significant mean shift; $K = 0.1785$, $x_f = 0.25$, $l_w = 10\ m$, $U_1(t=0) = 0.5$, $U_{m\neq1}(t=0) = 0$ and $P_m(t=0) = 0$.

right due to the steady base flow from left to right. Also, note that in figure 8(*c*) the streaming velocity is towards the cylinder along the direction of the propagation of the sound waves (*X* direction). In the present case, the Strouhal number (*St*) and the streaming Reynolds number (Re_s) are calculated as

$$\left.\begin{aligned} St &= fl_c/\bar{u} = \delta/2M = 1/2\varepsilon = 1, \\ Re_s &= (u_a|_{x_f})_{max} 2l_c/\nu \sim 80, \end{aligned}\right\} \tag{5.1}$$

where $f = c_0/2l_a$ is the fundamental frequency of the natural duct mode. The experiments performed in the *St* and Re_s regimes (Andres & Ingard 1953) indicate that the steady streaming velocity is directed towards the cylinder in the direction of oscillation of the free-stream flow field. The same is observed in the present simulation, as shown in figure 8(*c*). Streaming velocity field obtained from the present simulation cannot be compared with the experiments with externally excited acoustic field, due to the presence of the global-acceleration term. The same term does not vanish even during limit cycles and therefore only qualitative behaviour of the streamlines corresponding to the streaming velocity field can be compared with the experiments in acoustic streaming (Andres & Ingard 1953).

A non-zero averaged mean flow, which appears above the steady base flow due to acoustic streaming, results in non-zero averaged unsteady heat transfer from the heater. Figure 8(*d*) shows the evolution of the unsteady, non-dimensional heat transfer rate (q, see § 3.6) from the heater. The unsteady heat transfer rate q eventually reaches a limit cycle for linearly unstable systems (§ 5.1.2) where the oscillations during the limit cycle are about a non-zero mean. Acoustic streaming leads to a shift in the mean value of q.

6. Summary and conclusions

An analysis of thermoacoustic instability in an electrically heated horizontal Rijke tube is performed. The analysis started with an examination of the conservation equations for fluid flow. In the limit of zero Mach number of the steady flow and compact size of the heat source compared to the acoustic length scale, the equations become stiff. Therefore, solving the governing system of equations by the CFD technique is a difficult task. Hence, an asymptotic analysis is performed, which gave further physical insight into the problem. The flow variables are expanded in powers of Mach number. The equations thus obtained are identified as governing equations for the acoustic and hydrodynamic zones. An additional non-trivial term that has serious consequences for the stability of the system appeared in the momentum equation for the hydrodynamic zone, which cannot be obtained without performing the asymptotic analysis. The additional term is the global-acceleration term, which acts as a pressure gradient applied from the acoustic zone onto the hydrodynamic zone.

Numerical results show two stability regimes. In the first regime, the system is linearly stable. In the second regime, the system is linearly unstable and the perturbations eventually reach a limit cycle. A bifurcation diagram is then obtained with the heater power as the control parameter. The effect of the global-acceleration term is investigated using bifurcation diagrams. The term acts as one of the coupling terms (the other one is from the boundary condition for the momentum equation in the hydrodynamic zone) from the acoustic to the hydrodynamic zone. Therefore, the absence of the same term weakens the coupling between the acoustic and hydrodynamic zones. Without the global-acceleration term, the transition from

linearly stable to unstable behaviour occurs for a value of the non-dimensional heater power, which is one order of magnitude higher than the value of the heater power corresponding to the simulation with the above term. Thus, the linear stability of the system is predicted incorrectly in the absence of the term. The same term appears due to the two length-scale nature of the Rijke tube system, which is generic in thermoacoustic systems. The numerical computation of response functions in the past did not take into account the global-acceleration term. Hence, the evaluation of the stability of thermoacoustic system using the response function has to be performed carefully in the future.

Finally, the flow field during limit cycle oscillation is analysed. The limit-cycle amplitude is observed to be comparable to the steady base flow. Flow reversal occurs in the hydrodynamic zone during part of the limit-cycle oscillation. This nonlinear behaviour of the unsteady flow is observed as acoustic streaming during the limit cycle. A mean shift in the unsteady heat release rate from the heater is observed due to acoustic streaming.

In brief, asymptotic analysis gives the correct system of equations for the dynamics of the acoustic field and the heater. Also, using any response functions for the dynamics of the heater without rigorous mathematical arguments can lead to incorrect governing equations, which will lead to erroneous results.

The present variable density formulation was presented after an anonymous reviewer pointed out the errors in the constant density assumption adopted in an earlier version of the paper. The authors are grateful to the reviewer for the same. The authors thank C. Balaji, Professor S. R. Chakravarthy (Indian Institute of Technology Madras) and Professor W. Polifke (Technische Universität München) for their suggestions and interesting discussions during the study. This work was funded by the Department of Science and Technology (DST), India. The authors also thank Indian Institute of Technology Madras for providing access to the High Performance Computing Environment (HPCE).

Appendix. Governing equations and boundary conditions in the hydrodynamic zone

An unsteady heat transfer problem is solved with the system of equations (4.6). The heater, in its primitive form, is a thin wire filament wound around the heater frame. The heater wire filament is arranged in the form of a rack (a schematic diagram of the same is shown in figure 9*a*). The typical spacing between the racks of the wire filament is 50 times larger than the wire radius (∼mm). Hence, a two-dimensional flow over a single cylinder is considered, as shown in figure 9(*b*). The heat transfer from the single cylinder is multiplied by the effective length of the wire filament l_w to obtain the total heat transfer from the hydrodynamic zone.

A typical Reynolds number Re_d $(=2Re_c)$ of the base flow, based on the diameter of the wire filament, is around 20. Also, it is observed from figure 3(*a*) that the maximum non-dimensional acoustic velocity at the heater location u_f is approximately four. The fluctuating flow over the heater wire experiences a free-stream flow with a maximum flow velocity of five times the base flow during one cycle. Hence, the maximum Reynolds number (Re_m) to be obtained is 100 during one cycle. Sarpkaya (1986) experimentally obtained the condition for the above oscillatory flow to become unstable and shed vortices based on the non-dimensional number; Keulegan–Carpenter number K_c $(K_c = U_m T/D)$ for a given viscous scale parameter

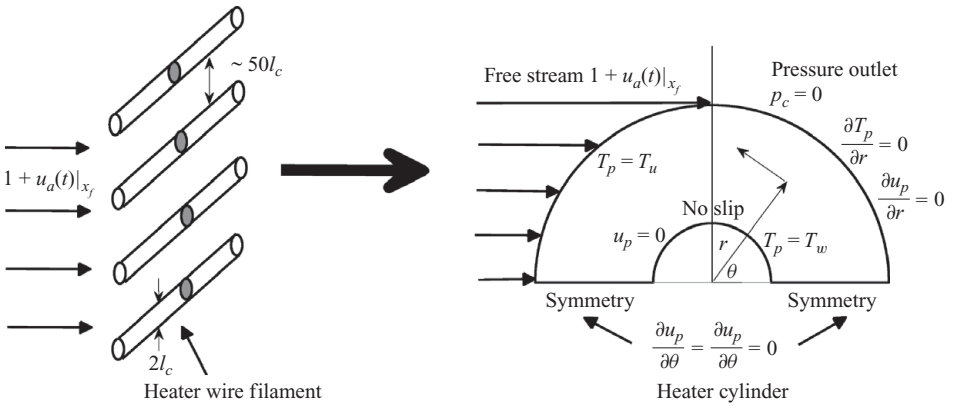

FIGURE 9. Schematic representation of the heat source: (*a*) rack of the heater wire filament; (*b*) boundary conditions for the two-dimensional flow over a heated circular cylinder.

β ($\beta = Re_m/K_c$), where U_m is the maximum velocity of the free stream encountered during a cycle and T is the time period of oscillation. For the present problem (parameter values from table 1), the values of the above non-dimensional numbers are $K_c = 1.25$ and $\beta = 80$. For $\beta = 80$, the critical value of K_c, above which the oscillatory flow over the cylinder becomes unstable to shed vortices, is 2.11 (Sarpkaya 1986), which is larger than that investigated in the present case. Hence, vortex shedding does not occur. Owing to this, only one half of the flow domain is considered for the present simulation and the symmetry boundary condition is enforced.

A plane polar coordinate system is used to implement the no-slip boundary condition on the surface of the wire filament (circular cylinder). Moreover, fluid viscosity and thermal conductivity are assumed to be independent of temperature. The flow domain and the boundary conditions are shown in figure 9(*b*). The switch from Dirichlet to Neumann boundary condition at $\theta = \pi/2$ (from upstream to downstream in figure 9*b*) for u_p, T_p is to have the numerical solvability of the hydrodynamic equations. The above switch is performed in Abu-Hijleh (2003) for a similar problem. The Dirichlet boundary condition (specified by the upstream acoustic zone) is applied in the far-field upstream boundary and the Newmann boundary condition is applied in the far-field downstream boundary for ρ_p, u_p and T_p. The average of the above flow variables in the downstream boundary of the hydrodynamic zone is used in the one-dimensional acoustic zone downstream of the heat source.

Near the cylinder surface, the gradient is large and it is important to cluster more grids near the cylinder surface. Therefore, grid clustering is incorporated by the transformation $r = e^{k\xi}$, where k is the grid clustering parameter, which determines the rate at which the grid grows as one moves away from the cylinder surface.

A uniform grid in the ξ, θ plane (computational plane) will give a stretched grid in the r, θ plane (physical plane). Figure 10(*a*) shows the generated grid for the present problem, where the grid size near the cylinder surface is very small compared to the far field and the grid size increases exponentially as r increases. The corresponding grid in the computational domain is uniform and is shown in figure 10(*b*). The system of equations (4.6) with the above transformation is solved by using semi-implicit method for pressure linked equation (SIMPLE) algorithm (Patankar 1980) with a fast Poisson solver (Press *et al.* 2007) for solving the pressure correction equation in the SIMPLE algorithm.

Property	$Re_d = 20$	$Re_d = 30$
Recirculation zone length (in terms of $2l_c$)	1.24 (1.15)	1.54 (1.54)
Separation angle from trailing edge (in radians)	0.79 (0.78)	0.87 (0.87)
Nusselt number $\left(Nu_d = \dfrac{2\tilde{T}_0^u}{2\pi(\tilde{T}_w - \tilde{T}_0^u)}\left[\left(\displaystyle\int_0^{2\pi}\left(-\frac{\partial T_p}{\partial r}\right)_{r=1} \mathrm{d}\theta\right)\right]\right)$	2.50 (2.40)	2.98 (2.83)

TABLE 2. Comparison of the steady-state flow properties between the present simulation and experiments. Numerical values in parentheses indicate values obtained from experiments. Experimental results for the recirculation zone length and the separation angle are obtained from Coutanceau & Bouard (1977), while the Nusselt number is obtained from Collis & Williams (1959).

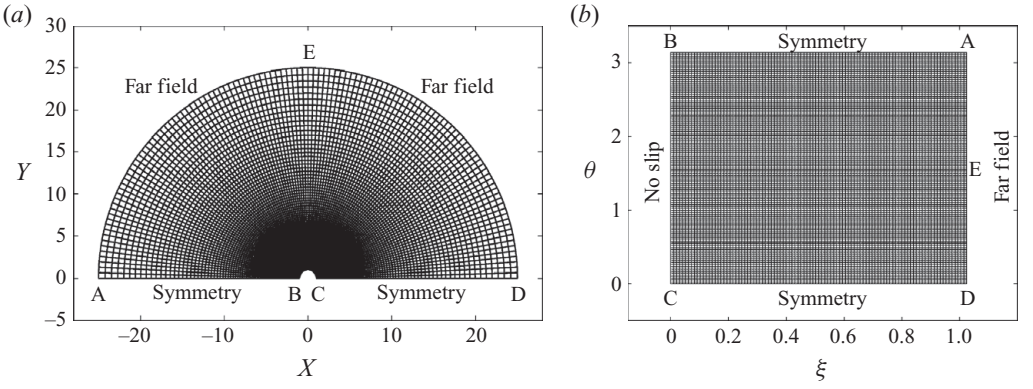

FIGURE 10. Grid generated (121×101) for flow in the hydrodynamic zone. (*a*) Physical domain with grid clustering near the cylinder surface with $k = \pi$. The flow domain is shown only up to $r = 25$ so that the presence of the cylinder can easily be visible in the figure. Numerical simulations are performed for the domain size $r = 50$. Convergence tests are performed and it is found that there is less than 5 % change in the results with the domain size for $r = 50$. (*b*) Computation domain with uniform grids.

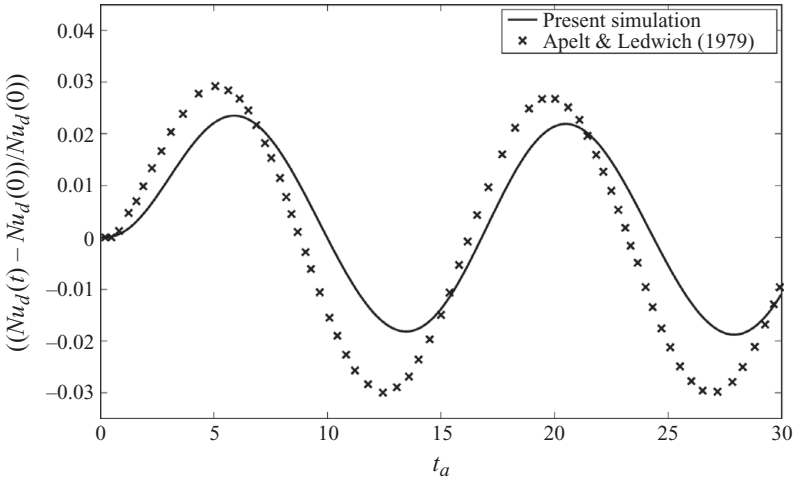

FIGURE 11. Response of the unsteady heat transfer from the heated cylinder for the forcing of the free-stream velocity, $u_p(r \to \infty, \pi/2 < \theta \leqslant \pi) = 1 + 0.1\sin(t_a/2.43)$. The parameters are $Re_d = 10$, $\tilde{T}_u = 295$ K and $\tilde{T}_w = 700$ K.

The results in the present numerical simulation (without the global-acceleration term) of the hydrodynamic zone are compared with the existing results for validation. The steady-state properties are compared in table 2 with experimental results from Coutanceau & Bouard (1977) and Collis & Williams (1959). Good agreement (with less than a 10 % difference) is observed for the steady-state properties. The response of the unsteady heat transfer from the heated cylinder to sinusoidal forcing is compared with the numerical simulation performed by Apelt & Ledwich (1979) and is shown in figure 11. Reasonable agreement in the response of the system is observed. The constant density formulation used by Apelt & Ledwich (1979) might be the reason for the difference in the above two responses of the unsteady heat release rate.

REFERENCES

Abu-Hijleh, B. A. K. 2003 Numerical simulation of forced convection heat transfer from a cylinder with high conductivity radial fins in cross-flow. *Intl J. Therm. Sci.* **42** (8), 741–748.

Anderson, J. D. 2001 *Computational Fluid Dynamics: The Basics with Applications*, 8th edn. McGraw-Hill.

Andres, J. M. & Ingard, U. 1953 Acoustic streaming at low Reynolds numbers. *J. Acoust. Soc. Am.* **25**, 932–938.

Apelt, C. J. & Ledwich, M. A. 1979 Heat transfer in transient and unsteady flows past a heated circular cylinder in the range $1 \leqslant Re \leqslant 40$. *J. Fluid Mech.* **95** (4), 761–777.

Balasubramanian, K. & Sujith, R. I. 2008 Thermoacoustic instability in a Rijke tube: Non-normality and nonlinearity. *Phy. Fluids* **20**, 044103.

Bittanti, S., Marco, A. D., Poncia, G. & Prandoni, W. 2002 Identification of a model for thermoacoustic instabilities in a Rijke tube. *IEEE Trans. Control Syst. Technol.* **10**, 490–502.

Candel, S. 2002 Combustion dynamics and control: Progress and challenges. *Proc. Combust. Inst.* **29** (1), 1–28.

Carvalho, J. A., Ferreira, M. A., Bressan, C. & Ferreira, L. G. 1989 Definition of heater location to drive maximum amplitude acoustic oscillations in a Rijke tube. *Combust. Flame* **76**, 17–27.

Collis, D. C. & Williams, M. J. 1959 Two-dimensional convection from heated wires at low Reynolds numbers. *J. Fluid Mech.* **6** (3), 357–384.

Coutanceau, M. & Bouard, R. 1977 Experimental determination of the main features of the viscous flow in the wake of a circular cylinder in uniform translation. Part 1. Steady flow. *J. Fluid Mech.* **79** (2), 231–256.

Culick, F. E. C. 2006 Unsteady motions in combustion chambers for propulsion systems. *Tech. Rep.* AG-AVT-039. RTO AGARDograph.

Fu, W. S. & Tong, B. H. 2002 Numerical investigation of heat transfer from a heated oscillating cylinder in a cross flow. *Intl J. Heat Mass Transfer* **45** (14), 3033–3043.

Hantschk, C. C. & Vortmeyer, D. 1999 Numerical simulation of self-excited thermoacoustic instabilities in a Rijke tube. *J. Sound Vib.* **227**, 511–522.

Heckl, M. A. 1990 Nonlinear acoustic effects in the Rijke tube. *Acustica* **72**, 63–71.

Heckl, M. A. & Howe, M. S. 2007 Stability analysis of the Rijke tube with a Green's function approach. *J. Sound Vib.* **305**, 672–688.

Kaufmann, A., Nicoud, F. & Poinsot, T. 2002 Flow forcing techniques for numerical simulation of combustion instabilities. *Combust. Flame* **131** (4), 371–385.

Klein, R. 1995 Semi-implicit extension of a Godunov-type scheme based on low Mach number asymptotics. Part I. One-dimensional flow. *J. Comput. Phys.* **121**, 213–237.

Klein, R., Botta, N., Schneider, T., Munz, C. D., Roller, S., Meister, A., Hoffmann, L. & Sonar, T. 2001 Asymptotic adaptive methods for multi-scale problems in fluid mechanics. *J. Engng Math.* **39**, 261–343.

Kopitz, J. & Polifke, W. 2008 CFD based application of the Nyquist criterion to thermoacoustic instabilities. *J. Comput. Phys.* **227**, 6754–6778.

Kwon, Y. P. & Lee, B. H. 1985 Stability of the Rijke thermoacoustic oscillation. *J. Acoust. Soc. Am.* **78**, 1414–1420.

Matveev, K. I. & Culick, F. E. C. 2003*a* A model for combustion instability involving vortex shedding. *Combust. Sci. Technol.* **175** (6), 1059–1083.

Matveev, K. I. & Culick, F. E. C. 2003*b* A study of the transition to instability in a Rijke tube with axial temperature gradient. *J. Sound Vib.* **264** (3), 689–706.

McManus, K., Poinsot, T. & Candel, S. 1993 A review of active control of combustion instabilities. *Prog. Energy Combust. Sci.* **19**, 1–29.

Moeck, J. P., Oevermann, M., Klein, R., Paschereit, C. O. & Schmidt, H. 2009 A two-way coupling for modeling thermoacoustic instabilities in a flat flame Rijke tube. *Proc. Combust. Inst.* **32** (1), 1199–1207.

Moeck, J. P., Schmidt, H., Oevermann, M., Paschereit, C. O. & Klein, R. 2007 An asymptotically motivated hydrodynamic-acoustic two-way coupling for modeling thermoacoustic instabilities in a Rijke tube. In *ICSV14, Cairns, Australia.*

Padmanabhan, M. S. 1975 The effect of nozzle nonlinearities on the nonlinear stability of liquid rocket motors. PhD thesis, Georgia Institute of Technology, Atlanta, USA.

Patankar, S. V. 1980 *Numerical Heat Transfer and Fluid Flow*. Hemisphere.

Poinsot, T. & Veynante, D. 2005 *Theoretical and Numerical Combustion*, 2nd edn. Edwards.

Preetham, Santosh, H. & Liewen, T. 2008 Dynamics of laminar premixed flames forced by harmonic velocity disturbances. *J. Propul. Power* **24** (6), 1390–1402.

Press, W. H., Teukolsky, S. A., Vetterling, W. T. & Flannery, B. P. 2007 *Numerical Recipes: The Art of Scientific Computing*, 3rd edn. Cambridge University Press.

Rayleigh, Lord. 1878 The explanation of certain acoustical phenomena. *Nature* **18**, 319–321.

Rienstra, S. W. & Hirschberg, A. 2004 *An Introduction to Acoustics*, IWDE 92-06 edn. Technische Universiteit Eindhoven.

Rijke, P. L. 1859 The vibration of the air in a tube open at both ends. *Phil. Mag.* **17**, 419–422.

Riley, K. F., Hobson, M. P. & Bence, S. J. 2006 *Mathematical Methods for Physics and Engineering*, 3rd edn. Cambridge University Press.

Sarpkaya, T. 1986 Force on a circular cylinder in viscous oscillatory flow at low Keulegan–Carpenter numbers. *J. Fluid Mech.* **165**, 61–71.

Selimefendigil, F., Föller, S. & Polifke, W. 2008 Nonlinear identification of the unsteady heat transfer of a cylinder in pulsating crossflow. In *Intl Conf. on Jets, Wakes and Separated Flows*. Technical University Berlin, Berlin, Germany.

Song, W. S., Lee, S., Shin, D. S. & Na, Y. 2006 Thermo-acoustic instability in the horizontal Rijke tube. *J. Mech. Sci. Technol.* **20**, 905–913.

Telionis, D. P. 1981 *Unsteady Viscous Flows*. Springer.

Ting, L., Klein, R. & Knio, O. M. 2007 *Vortex Dominated Flows: Analysis and Computation for Multiple Scales*, Series in Applied Mathematical Sciences. Springer.

Wu, X. & Moin, P. 2010 Large-activation-energy theory for premixed combustion under the influence of enthalpy fluctuations. *J. Fluid Mech.* **655**, 3–37.

Wu, X., Wang, M., Moin, P. & Peters, N. 2003 Combustion instability due to the nonlinear interaction between sound and flame. *J. Fluid Mech.* **497**, 23–53.

Zeytounian, K. H. 2002 *Asymptotic Modelling of Fluid Flow Phenomena*. Kluwer.

Zinn, B. T. & Lieuwen, T. C. 2006 *Combustion Instabilities: Basic Concepts – Combustion Instabilities in Gas Turbine Engines: Operational Experience, Fundamental Mechanisms, and Modeling*. AIAA.

Zinn, B. T. & Lores, M. E. 1971 Application of the Galerkin method in the solution of non-linear axial combustion instability problems in liquid rockets. *Combust. Sci. Technol.* **4**, 269–278.